

Original Research

Spatio-Temporal Variation Characteristics of Summer Precipitation in China and Its Response to ENSO

Yang Chen¹, Long Ma^{1*}, Tingxi Liu¹, Xing Huang¹, Guohua Sun²

¹College of Water Conservancy and Civil Engineering, Inner Mongolia Agricultural University, Hohhot 010018, China

²Hydrology and Water Resources Survey Centre of Bayannur, Inner Mongolia, Bayannur 015000, China

Received: 28 March 2023

Accepted: 16 June 2023

Abstract

This article was to reveal the spatio-temporal variation of summer precipitation in China and its response to El Niño-Southern Oscillation (ENSO). The results showed that the precipitation increased in 1900 s~1950 s, then decreased in 1960 s~1970 s, and increased in 1980 s~2010 s again. In space, it presented a "five-layered sandwich structure" featuring rising-falling-rising-falling-rising from northwest to southeast. The precipitation was generally less when ENSO occurred, but there were differences in intensities, regions, and so on. For example, When El Niño (all types) occurred, there was more precipitation in the western Continental Basin and the southern Huaihe River Basin, but less in the Yellow River Basin. When the extremely strong and medium La Niña occurred, the precipitation was more in the central and less in the north and the south. When the weak La Niña occurred, the precipitation increased in the northwest, decreased in the southeast, and vice versa for the extremely weak La Niña. Precipitation and Oceanic Niño Index (ONI) were negatively correlated in time, however, in space, there was a negative correlation in the north, and a positive correlation in the south, the dividing line was approximately at 29°N. In addition, the correlation between precipitation and ONI was proportional to the intensity of ENSO.

Keywords: precipitation, spatio-temporal variation, ENSO, response, China

Introduction

The ENSO is not only the strongest interannual oscillation in the earth's climate system, but also an important factor that indirectly affects precipitation through teleconnection between ocean and atmosphere, which has a significant impact on the climate in most

parts of the world, including China [1]. Therefore, discussing the relationship between summer precipitation anomalies and ENSO in China is one of the important research tasks at present [2].

Based on observational or dynamic simulation data, many scholars have used Complete Ensemble Empirical Mode Decomposition with Adaptive Noise [3], Partial wavelet coherence [4], Pearson correlation [5], Community Earth System Mode [6] and other methods to study the relationship between precipitation and ENSO in the Globe [7, 8], as well as South America

*e-mail: malong4444333@163.com

[9], central Asia [10,11], the tropical Pacific [12], Canada [13], the United States [14], Sapporo [15], and other places under the scale of month, season and year. The results showed that ENSO was the link between sea surface temperature anomalies and atmospheric anomalies in the tropical Pacific Ocean, which can not only affect the climate conditions in the tropical Pacific Ocean, but also cause precipitation anomalies, even large-scale extreme precipitation events globally [16] through teleconnection [17]. ENSO was also one of the main factors modulating precipitation in south America [9], Africa [18], and other places. Precipitation in spring, autumn and winter in Central Asia was highly correlated with ENSO with time delay [10]. When ENSO was in the positive/negative phase, there was obviously less/more precipitation in Canada [13]. while more/less precipitation in the Andes [19] and southern California [20]. Below (above) normal precipitation response to the El Niño events at the North-West region (South-West region, Middle-Inland region, South-East region, and North-East region), while the opposite patterns were detected for the cold phase of ENSO [14]. In Sapporo (located in northern Japan), more snow fell in the southwestern mountains and inland areas during El Niño winters, and more snow fell in the northeastern plains and along the sea during La Niña winters [15]. More August IndoChina Peninsula precipitation falls in La Niña developing years during 1959~1979, but in El Niño developing years during 1983~2003 [21].

Some scholars have also conducted several researches on the relationship between precipitation and ENSO in China. The results showed that the relationship between precipitation and ENSO in China had strong regional heterogeneity and time differences [22]. For example, the eastern Pacific El Niño events exhibit significant impacts on the extreme precipitation over the central and southern China during the developing autumn, resulting in increased extreme precipitation in southern China and decreased extreme precipitation in central China [23]. When the successive El Niño/La Niña events occurred, anomalously more snowfall in Guanzhong Plain [24]. The influence of ENSO on precipitation in eastern China was mainly in spring and winter [25]. The winter precipitation of south China was positively correlated with ENSO. The central summer precipitation was opposite to it [26]. The winter precipitation in southern China showed an upward trend in eastern Pacific (EP) El Niño years, and the opposite was true in EP La Niña years. Summer precipitation in EP El Niño years showed a three poles structure of rising in the north and south, but falling in center, while in central Pacific (CP) El Niño years, precipitation was mainly rising [27]. Many scholars have proposed that the correlation between precipitation and ENSO in China, including central [28,29], northwestern [30], northeastern [31], etc., was weak as a whole before the 1990s. After being affected by the change of the Philippine anticyclone [26], the warming of the tropical Indian Ocean [31], the

phase anomaly of the sea temperature, and the change of the walker circulation, it significantly intensified [28].

Existing relevant results demonstrated that precipitation had different sensitivities in response to different types of ENSO events [32]. Yet such sensitivities have not been quantified. Most of them were studies on the correlation between precipitation and ENSO [33], while the differences and connections in correlation between precipitation and ONI under the different types and intensities of ENSO events remain unclear.

Based on what has been mentioned above, to make the research results highly representative and comprehensive, this article took China as the study area, for it covers a vast expanse of land with a large number of climate types. Based on precipitation and SST raster data sets from January 1901 to December 2020, the response of precipitation to ENSO was comprehensively revealed, which can enrich the research results in this field and provides a reference for disaster prevention.

Materials and Methods

Study Area

The study area is China (73°33'E-135°05'E, 3°51'N-53°33'N), with a total area of about $9.6 \times 10^6 \text{ km}^2$ (Fig. 1), which can be divided into 9 major watersheds [34]: Songhua and Liaohe River Basin, Haihe River Basin, Huaihe River Basin, Yellow River Basin, Yangtze River Basin, Pearl River Basin, Southeast Basin, Southwest Basin and Continental Basin. The watershed boundary data was from Resource and Environment Science and Data Center.

Data Used

The precipitation data used was the raster data set of monthly precipitation at 1 km resolution in China, which came from "the national earth system science data center (<http://www.geodata.cn/>)" and was provided by Professor Peng Shouzhong's team of Northwest A&F University [35]. After inspection, the data can represent the precipitation conditions in the study area. In addition, the summer precipitation data used in this study was the sum of the precipitation in June, July, and August.

The ONI data used was divided into two parts. The first part was the Extended Reconstructed Sea Surface Temperature version 5 data set downloaded from National Oceanic and Atmospheric Administration (NOAA), after format conversion, extraction and other steps, the mean value of the sea surface temperature anomaly (SSTA) in the Niño 3.4 region from January 1901 to December 1950 was obtained, then the ONI was calculated. The second part of ONI data was downloaded directly from the NOAA. The time series started from January 1951 and ended in December

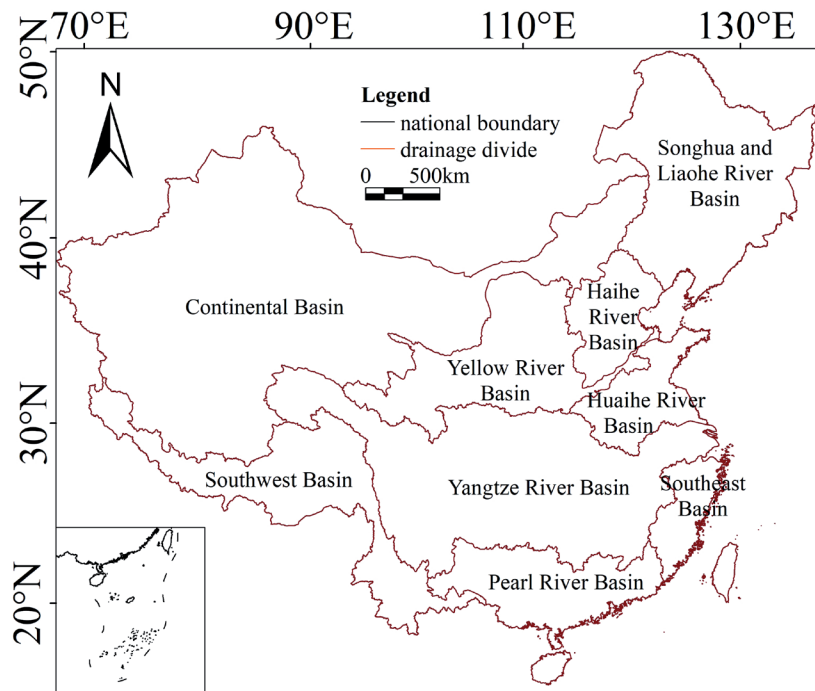


Fig. 1. Location of the study area.

2020. The total duration of the two parts data was 120 years. Both parts of data were from NOAA. The specific download address was: <https://www.ncdc.noaa.gov/telecon-nections/enso/enso-tech.php>.

Data Processing Methods

Arcgis software was used for coordinate transformation and extraction to obtain monthly data of precipitation and SSTA in the Niño 3.4 region, and the format of all data was unified as tiff.

(2) Based on the least squares method, the linear regression model was used to simulate the variation of precipitation in the study area on the basis of each pixel. The specific calculation formula is as follows [36]:

$$\theta = \frac{n \sum_{i=1}^n i c_i - \sum_{i=1}^n i \sum_{i=1}^n c_i}{n \sum_{i=1}^n i^2 - (\sum_{i=1}^n i)^2}$$

Where, θ is slope of summer precipitation (mm/10a), c_i is summer precipitation value in year i (mm), n is the length of study period, here was 120.

(3) The moving average method was used to conduct auxiliary analysis of the variation of precipitation. The specific calculation formula is [37]:

$$x = \frac{1}{n} \sum_{i=1}^n x_{j+n-1}$$

Where, n is sliding length, and the n value of this article was 11.

(4) the coefficient of variation was used to characterize the intensity of precipitation in the

study area, and the specific calculation formula is as follows:

$$CV = \frac{\sqrt{\frac{1}{n-1} \sum (x_i - \bar{x})^2}}{\bar{x}}$$

Where, CV is coefficient of variation, i is time series, x_i is the mean value of all pixel values during the study period.

In addition, according to the fluctuation degree of precipitation, CV was divided into five levels, which were: $CV > 4.8$ (high fluctuation), $3.6 < CV \leq 4.8$ (relatively high fluctuation), $2.4 < CV \leq 3.6$ (moderate fluctuation), $1.2 < CV \leq 2.4$ (relatively low fluctuation) and $CV < 1.2$ (low fluctuation).

(5) The Z test was used to identify the significance of precipitation change [38]. The specific calculation formula is:

$$S = \sum_{k=1}^{n-1} \sum_{j=k+1}^n Sgn(X_j - X_k)$$

$$Sgn(X_j - X_k) = \begin{cases} +1 (X_j - X_k > 0) \\ 0 (X_j - X_k = 0) \\ -1 (X_j - X_k < 0) \end{cases}$$

$$Z = \begin{cases} \frac{S-1}{\sqrt{V(S)}} & S > 0 \\ 0 & S = 0 \\ \frac{S+1}{\sqrt{V(S)}} & S < 0 \end{cases}$$

(6) Morlet wavelet, cross wavelet and wavelet coherence methods were used to analyze the precipitation cycle, and phase relationship between precipitation and ONI in all energy regions, which implemented by Matlab software, the theoretical formula is as follow [39-40]:

$$\varphi(K\omega) = \frac{\pi^{-\frac{1}{4}}H(\omega)e^{-(K\omega-\omega_0)^2}}{2}$$

Where, K is the wavelet scales, ω is frequency, $H(\omega) = Heaviside\ step\ function$, $H(\omega) = 1$, if $\omega > 0$, $H(\omega) = 0$, otherwise, ω_0 is the nondimensional frequency.

Then, the wavelet transform can be defined as:

$$\omega_f(\alpha, b) = |\alpha|^{-\frac{1}{2}} \int_R f(t) \varphi\left(\frac{t-b}{\alpha}\right) dt$$

Where, a and b are scale factor and time factor, respectively, $\omega_f(\alpha, b)$ is a wavelet transform coefficient, $\varphi_{a,b}(t)$ is a function obtained by scaling and translating, $\varphi(t)$:

$$\omega_{\alpha,b} = |\alpha|^{-\frac{1}{2}} \varphi\left(\frac{t-b}{\alpha}\right)$$

Where, $\alpha > 0$, and $b \in \mathbb{R}$.

The distribution of wave energy with scale factor a can be measured by wavelet variance:

$$Var(\alpha) = \int_{-\infty}^{+\infty} \omega_f(\alpha, b)^2 db$$

The wavelet variance facilitates the analysis on the main periods of each sequence.

The wavelet energy spectrum can be defined as:

$$W_X(\alpha, \tau) = C_X(\alpha, \tau)C_X^*(\alpha, \tau) = |C_X(\alpha, \tau)|^2$$

Where, $C_X(\alpha, \tau)$ is the wavelet transform coefficient of sequence $x(t)$, $*$ is the complex conjugate. The wavelet energy spectrum can be used to identify the multiscale evolution and mutation features of sequences.

Extended from the traditional wavelet analysis, the Cross Wavelet Transform (XWT) is a novel technique to analyze multiple signals on various scales. The XWT can effectively evaluate the correlation degree between two sequences, and reflect the phase structure and details of the sequences in time domain and frequency domain. The cross wavelet spectrum of sequences $x(t)$ and $y(t)$ can be defined as:

$$W_{XY}(\alpha, \tau) = C_X(\alpha, \tau)C_Y^*(\alpha, \tau)$$

The absolute value $|W_{XY}|$ of the cross wavelet spectrum is the energy spectrum of cross wavelet.

Different spectra have the following relationship:

$$\left(\frac{|W_n^X(s)W_n^{Y*}(s)|}{\sigma_X\sigma_Y} < p\right) = \frac{Z_v(p)}{v} \sqrt{P_k^X P_k^Y}$$

Where, $PX\ k$ and $PY\ k$ are the background power spectra of sequences X and Y , respectively, σ_X and σ_Y are the standard deviations of sequences X and Y , respectively, $Z_v(p)$ is the confidence coefficient related to probability p , v is the degree of freedom.

The degree of coherence of wavelet transform can be expressed as:

$$R^2(\alpha, \tau) = \frac{|S(\alpha^{-1}W_{XY}(\alpha, \tau))|^2}{S(\alpha^{-1}|W_X(\alpha, \tau)|^2)S(\alpha^{-1}|W_Y(\alpha, \tau)|^2)}$$

Where: S is a smoothing operator.

In the time-frequency domain, the degree of coherence between two wavelet transforms can be demonstrated by wavelet coherence spectrogram, where the phase spectrum reflects the response and lag between two sequences, and the phase angle reveals the direction of correlation of two sequences.

(7) For the correlation between precipitation and ONI, the pearson correlation coefficient between precipitation and ONI was calculated, the formula is as follow [41]:

$$R_{xy} = \frac{\sum_{i=1}^n (x_i - \bar{x})(y_i - \bar{y})}{\sqrt{\sum_{i=1}^n (x_i - \bar{x})^2 \sum_{i=1}^n (y_i - \bar{y})^2}}$$

Where, x_i is value of precipitation in year i , y_i is value of ONI in year i , \bar{x} is multi-year mean value of precipitation, \bar{y} is multi-year mean value of ONI, n is the number of years.

Definition and Dividing Criterion of ENSO Events

According to the definition of ONI and ENSO given by NOAA: ENSO is a phenomenon in the equatorial Pacific Ocean characterized by a five consecutive 3 month running mean of SST anomalies in the Niño 3.4 region that is above (below) the threshold of +0.5°C (-0.5°C). This standard of measure is known as the Oceanic Niño Index. On the basis of this standard, a total of 29 El Niño events and 38 La Niña events were identified this time, and each type of event occurred once every 4 to 5 years [43].

Based on previous research results [44], this article divided ENSO events into two categories and 10 subcategories with intensity: El Niño/La Niña extremely strong type (EES/LES), El Niño/La Niña strong type (ES/LS), El Niño/La Niña medium type (EM/LM), El Niño/La Niña weak type (EW/LW), and El Niño/La Niña extremely weak type (EEW/LEW).

Results and Discussion

Results

Spatial and Temporal Variation of Precipitation

Fig. 2 showed the temporal evolution of the regional mean value of precipitation a), the spatial distribution of the multi-year mean value of precipitation b), the slope of precipitation c), the CV of precipitation, d) and its cycle (e~f) in turn. The precipitation increased (1900s~1950s) first, then decreased (1960s~1970s), and increased (1980s~2010s) again. The multi-year mean value of precipitation in the study area was 294.15 mm.

The maximum value of precipitation appeared in 1998 (347.50 mm), and the minimum value appeared in 1972 (255.20 mm). In terms of space, the maximum value of precipitation distributed in the Southeast Basin and the Pearl River Basin in China. As a whole, the average precipitation of the region exceeded 700 mm, while the minimum one was concentrated in the middle of the Continental Basin, mostly less than 100 mm. The overall precipitation was increasing from northwest to southeast China. The overall summer precipitation in the study area was increased, accounting for 63.1% of the study area (hereinafter referred to as "area with increasing precipitation", otherwise referred to as "area with decreasing precipitation"), which was mainly distributed

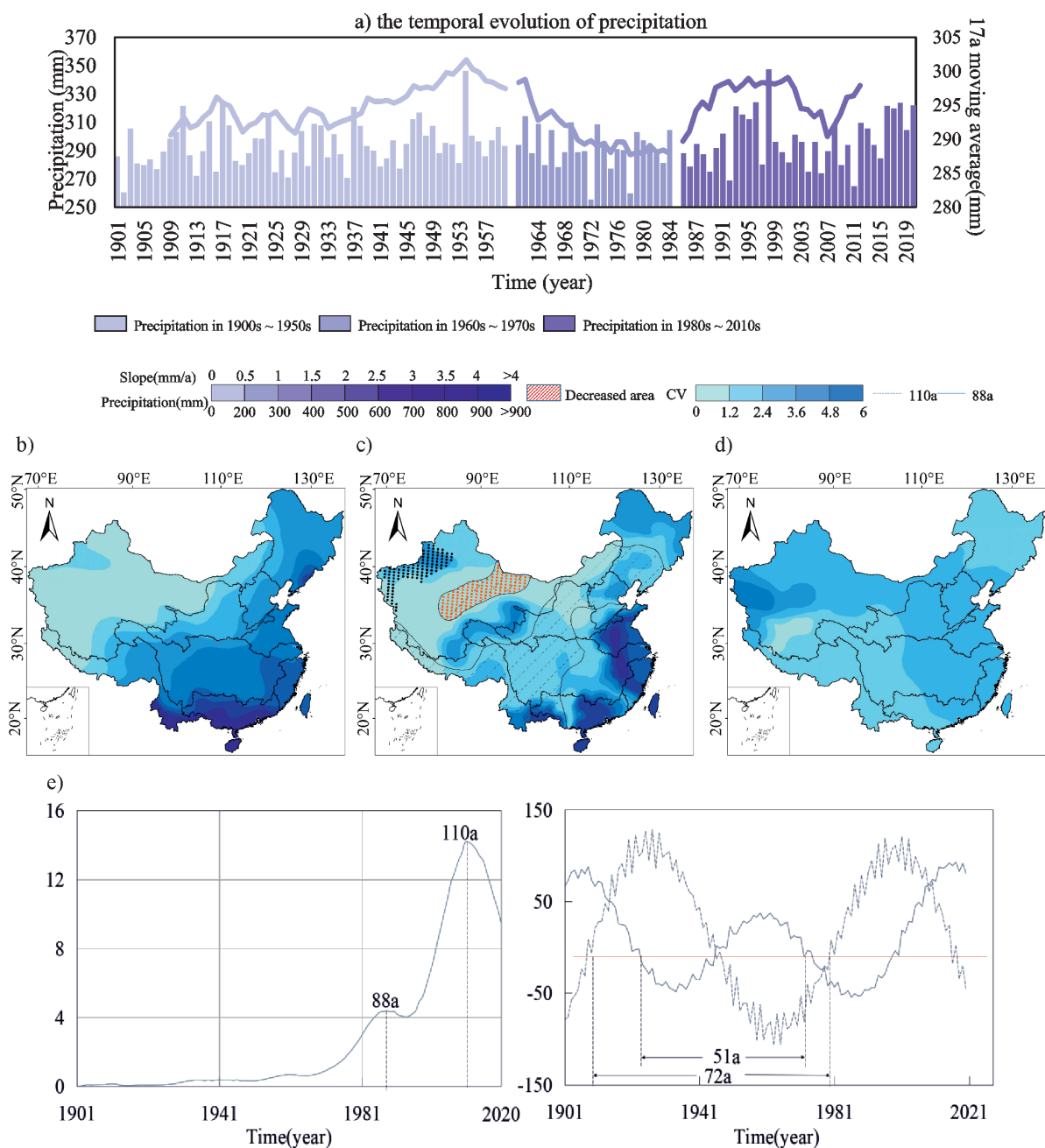


Fig.2. The spatial distribution of summer precipitation, slope and CV in the study area and its period.

in the Continental Basin, the Songhua and Liaohe River Basin, the Huaihe River Basin, the Southeast Basin, the Pearl River Basin and other places in China. Among them, the precipitation of the northwest part of the Continental Basin rose most significantly, which passed the significance test of 95% confidence. This may be caused by the melting of icebergs due to global warming. The fluctuation of precipitation in the area with increasing precipitation was generally large. Specifically, except the Songhua and Liaohe River Basin, which belonged to the relatively low fluctuation area, most of the other areas belonged to the medium fluctuation area or relatively high fluctuation area, and the small area in the western part of the Continental Basin even belonged to the high fluctuation area, with the *CV* exceeded 4. The precipitation of 36.9% of the regions dropped in summer, but the downward trend was not significant, and the decrease rate was mostly between 0 and 2.5 mm/a. Only 15.5% of the regions passed the significance test of 95% confidence, which was mainly concentrated in the northeast part of the Continental Basin. The overall fluctuation of precipitation in the area with decreasing precipitation was small, and thus this area belonged to the low fluctuation area or the relatively low fluctuation one.

The oscillation period of the summer precipitation series in the study area was the most obvious around 110a and 88a, that was, there was the 110a first main cycle and the 88a second main cycle, both of which were full time domain oscillations. Under the time scale of 110a, there was a 74a cycle, and there were two obvious flood centers in 1927 and 2001, with one drought center in 1965. There was a 51a cycle in the 88a time scale, with three flood centers (1908, 1959 and 2017) and two drought centers (1934 and 1986)

Variation Characteristics of ENSO Events

The occurrence of ENSO events in recent a hundred years had obvious interdecadal characteristics. It can be seen from the Fig. 3 that the frequency of El Niño events increased over time. The frequency of EM was the highest, accounting for about one-third of the total, followed by EW and EEW, and both EES and ES occurred three times. The frequency of La Niña was opposite to that of El Niño on the whole. The frequency of LES was the highest, accounting for more than 40% of the total frequency of La Niña, followed by LM, LW, and LS. The frequency of LEW was the lowest, which only occurred twice (2008 and 2016). In consideration of factors such as the occurrence time and duration of ENSO, only 13 El Niño events and 22 La Niña ones were selected for this analysis.

Response Relationship between Precipitation and El Niño

Fig. 4 showed the spatial distribution of percentage of summer precipitation anomalies (it can be divided

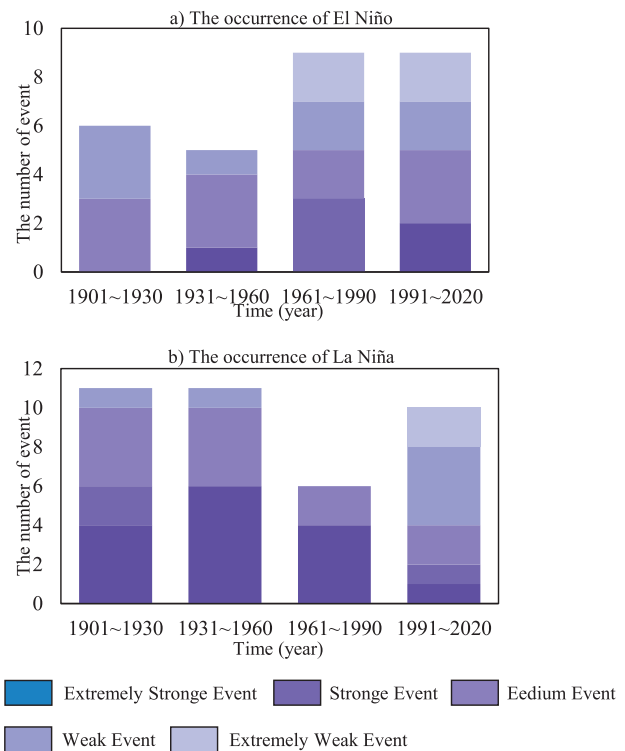


Fig. 3. Number of occurrences of ENSO events.

into the percentage increase of summer precipitation and the percentage decrease of summer precipitation, abbreviated as PISP and PDSP, respectively, the same below) in China under El Niño event with different intensity. When an EES occurred, the areas with more precipitation and less precipitation in the study area were nearly equivalent, accounting for 43.5% and 56.5% of the total study area, respectively. Among them, the areas with more precipitation were mainly concentrated in the western part of the Continental Basin, and the PISP was roughly 30%. There was also more precipitation on the two sides of the Qinling-Huaihe line as a whole, forming an eastward-westward "rain band", but the PISP was small, precipitation increased by only 5%~12% here. The regions with less precipitation were mainly concentrated in the Yellow River Basin. Compared with the normal year, there was less precipitation in 12.9% of the total study area, the reduction of which was up to 20% or more. When the ES and EM events occurred, the summer precipitation in the study area was generally less, accounting for 68.0% and 62.8% of the study area, respectively. Among them, in the year when the ES occurred, the regions with less precipitation were mainly distributed in the Yellow River Basin and the northeast of the Continental Basin, The PDSP was between 20% and 29%. When EM occurred, except for the Southwest Basin, there was more precipitation in the west of the study area generally (took the Continental Basin as an example, the PISP in the Continental Basin was mostly between 30%~40%) and less precipitation in the east (the overall PDSP in the east of the Yellow River Basin was more than 20%). When EW occurred, the area

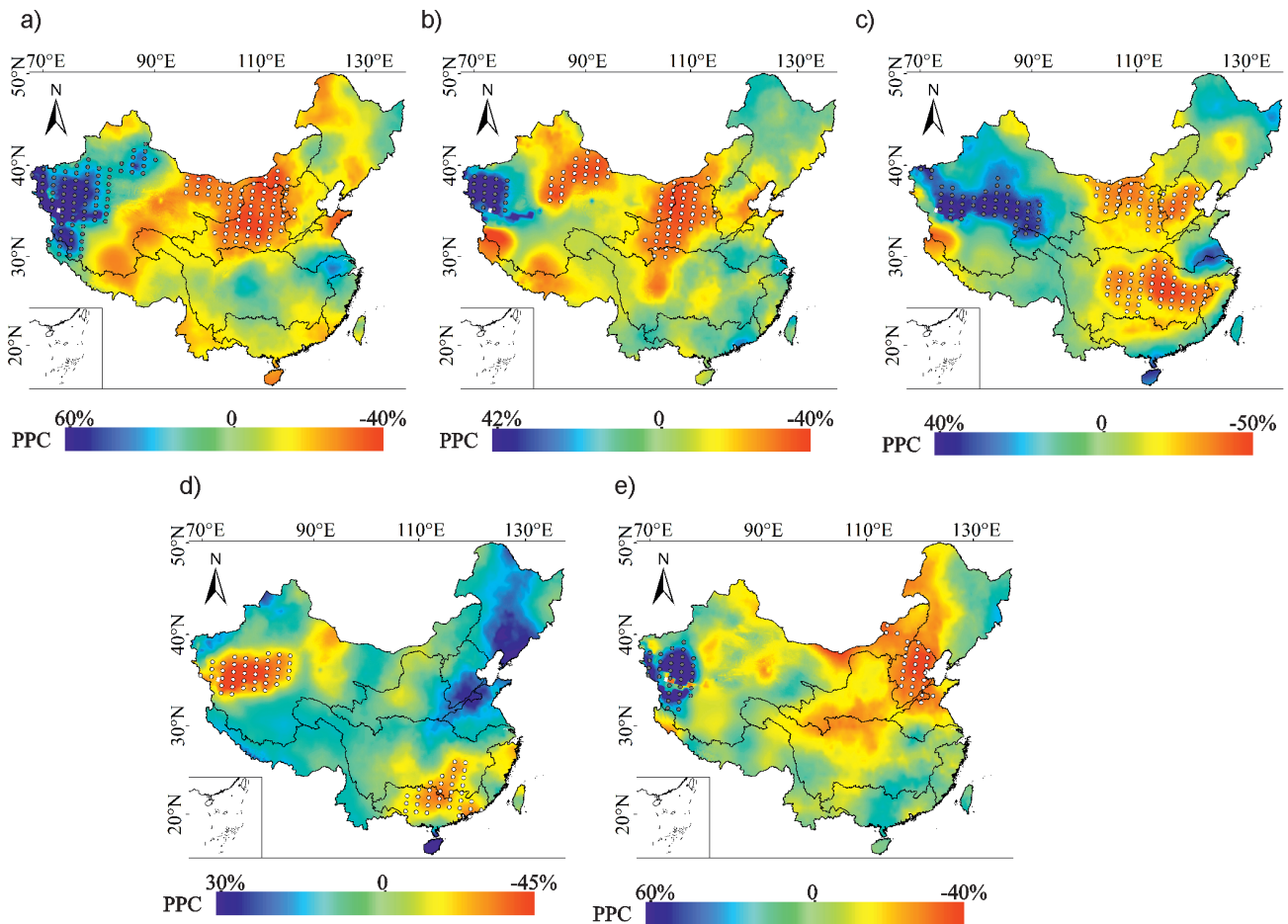


Fig. 4. Percentage change of precipitation in different types of El Niño. Note: The dots in the figure were the areas where the percentage of precipitation change (PPC) exceeded 20%, as follows.

with more precipitation in the study area accounted for roughly one-third of the total, mainly concentrated in the Songhua and Liaohe River Basin, the Haihe River Basin and the Southwest Basin in China. Among them, the PISP in the Songhua and Liaohe River Basin and the Haihe River Basin increased from north to south, with a range of 10%~20%, while the PISP in the Southwest Basin was relatively small, mostly less than 5%. The areas with less precipitation accounted for 65.5% of the total study area. However, except for the central and western part of the Continental Basin and the junction of the Pearl River Basin and the Yellow River Basin, there were few changes in the precipitation in other areas, with the PDSP mostly between 4% and 10%. There was more precipitation in the study area in summer in the year when the EEW occurred, accounting for 53.7% of the total study area. The area with more precipitation was mainly distributed in the western part of the Continental Basin, and the PISP was more than 20% of the multi-annual average. The areas with obvious less precipitation were mainly concentrated in the central and western parts from the Songhua and Liaohe River Basin to the Haihe River Basin and the "northeast-southwest" rain band with low precipitation in the Yangtze River Basin, with the PDSP between 7% and 20%.

Response Relationship between Precipitation and La Niña

Fig. 5 showed the spatial distribution of the percentage of summer precipitation anomalies in China under La Niña event with different intensity. It can be seen from Fig. 5 that, in the year when the LES occurred, the areas with more or less precipitation accounted for 49.8% and 50.2% of the total study area, respectively. There was less precipitation in the north and the south, and more precipitation in the middle. In terms of the overall spatial pattern, the areas with more precipitation were mostly distributed around 30°N (hereinafter referred to as "30°N rain band"). In the 30°N rain band, the PISP was the lowest in the west of the Yangtze River Basin, and increased in the east and west sides. The PDSP in the north of the 30°N rain band was the largest in the east of the Songhua and Liaohe River Basin and the west of the Continental Basin, and gradually decreased toward the middle of the study area. The PDSP in the south of the rain band was the largest in the southern part of the Pearl River Basin, and gradually decreased to the east and west sides. When LS occurred, the area with less precipitation in the study area accounted for about 55.8%, mainly distributed in the Songhua

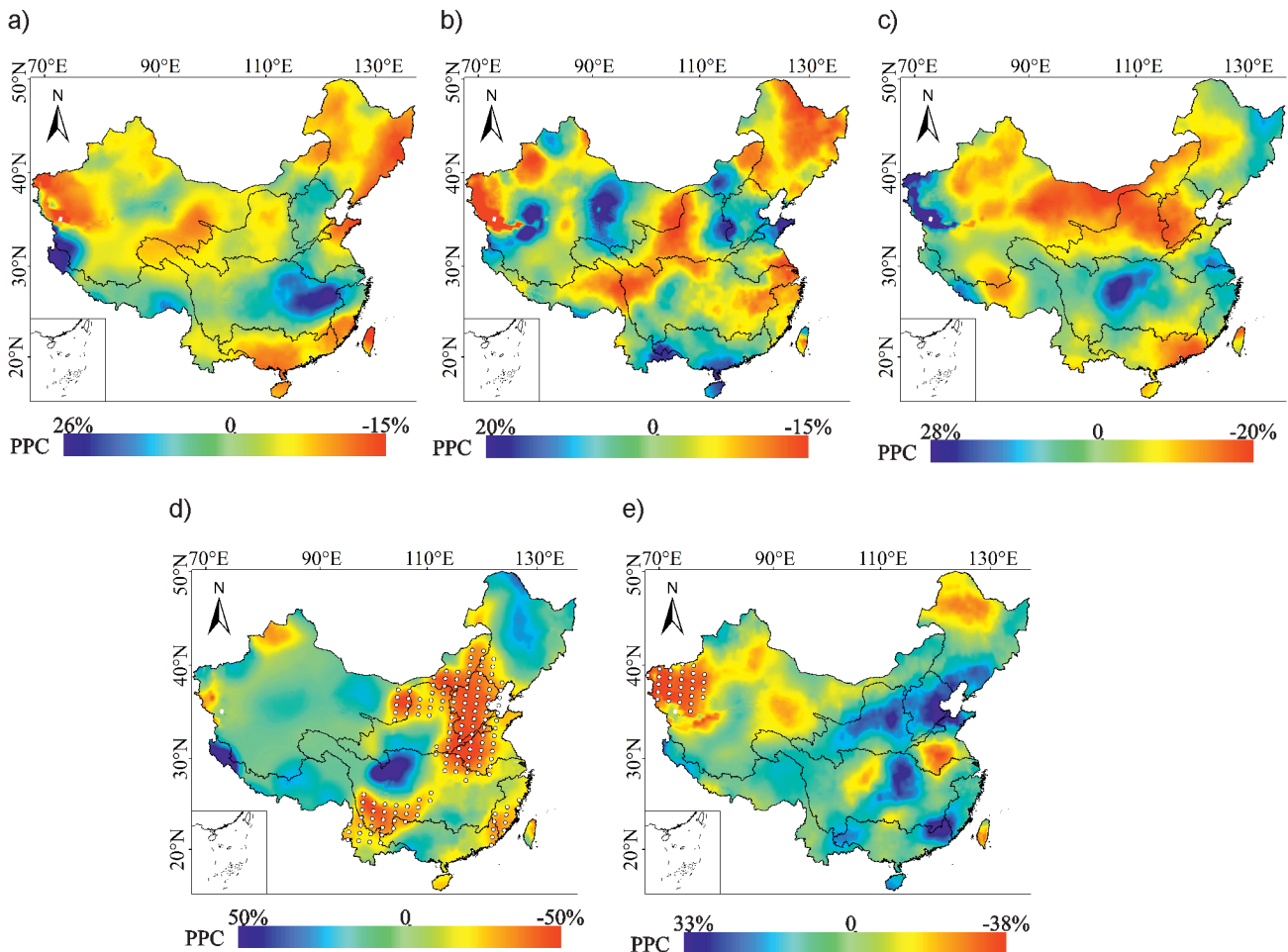


Fig.5. Percentage change of precipitation in different types of La Niña.

and Liaohe River Basin, the central and western Yellow River Basin, and the junction of the Huaihe River Basin and the Yangtze River Basin. Among them, the PDSP in the Songhua and Liaohe River Basin was 10%~13.5%, and other regions was less than 10%. The regions with more precipitation were mainly concentrated in the southeastern Continental Basin, the Haihe River Basin and the Pearl River Basin, among which, the southeastern Continental Basin had the highest PISP (mostly between 11.5% and 17%), followed by the Haihe River Basin and the Pearl River Basin (less than 10% overall). When the LM occurred, the precipitation in the study area generally showed a sandwich structure of less-more-less precipitation from north to south, and the areas with more or less precipitation accounted for 38.1% and 61.9% of the total study area, respectively. Among them, except for the western part of the Continental Basin, where the PISP was more than 12%, the rest of the areas were less than 10%, and there was a small change in the area with less precipitation in the middle of the study area, increased to the south and north. When the LW and the LEW occurred, the precipitation in the study area was less on the whole (accounted for 64.0% and 60.4% of the total study area, respectively). The difference was that when the LW occurred, there was more precipitation

in the northwest and less in the southeast. Among them, the regions with less precipitation were mainly distributed in the Haihe River Basin, the west of the Huaihe River Basin and the south of the Yangtze River Basin, and the PDSP was more than 20%. The regions with more precipitation were mainly concentrated in the middle of the Continental Basin and the Southwest Basin, yet the PISP was small, most of which was less than 10%. Except for the central part of the Huaihe River Basin (where there was less precipitation), the spatial distribution of precipitation in the study area in the year of the LEW was roughly opposite to that of the LW, and only the PDSP in the western part of the Continental Basin exceeded 20%. The PDSP in the rest of the regions were all less than 15%.

Correlation and Correspondence between Precipitation and ENSO

Fig. 6 were the cross wavelet and wavelet transform analysis results of summer precipitation and ONI respectively. It can be discovered that summer precipitation and ONI have significant resonance stages in the both high and low energy regions (mainly in the 2~8a period). Among them, the significant resonance

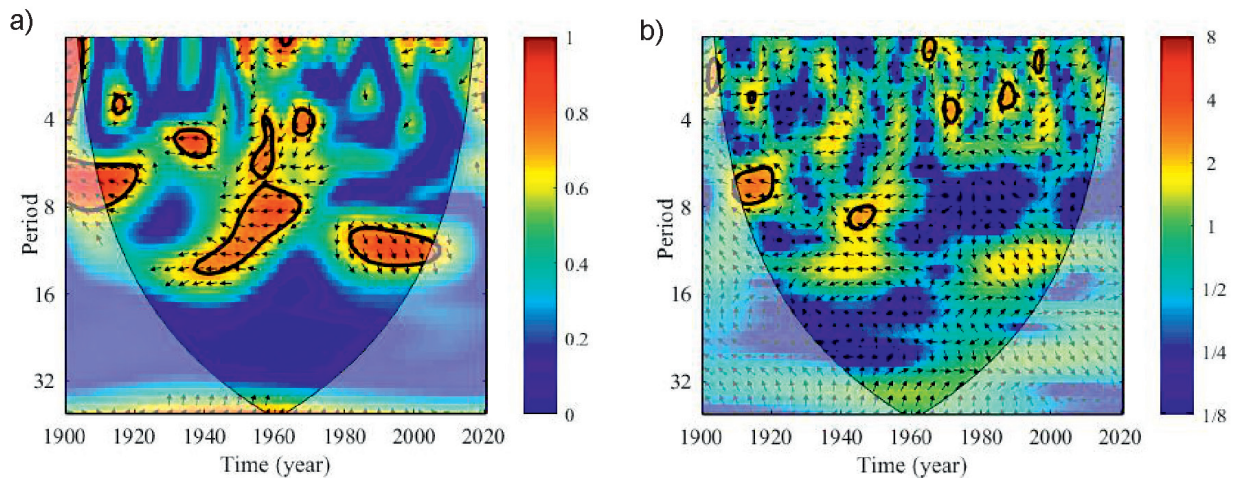


Fig. 6. Cross wavelet and wavelet transform analysis of summer precipitation and ONI.

stage in the high-energy region was mainly reflected in the period from 1908 to 1920, and the two phases were positively correlated in the corresponding frequency bands during this stage; There were two significant resonance stages in the low-energy region, which

were 1940~1968 and 1980~2000, and the former was negatively correlated (precipitation and ONI) and the latter was positive.

Fig. 7 showed the spatial distribution of the correlation coefficients between precipitation and ONI

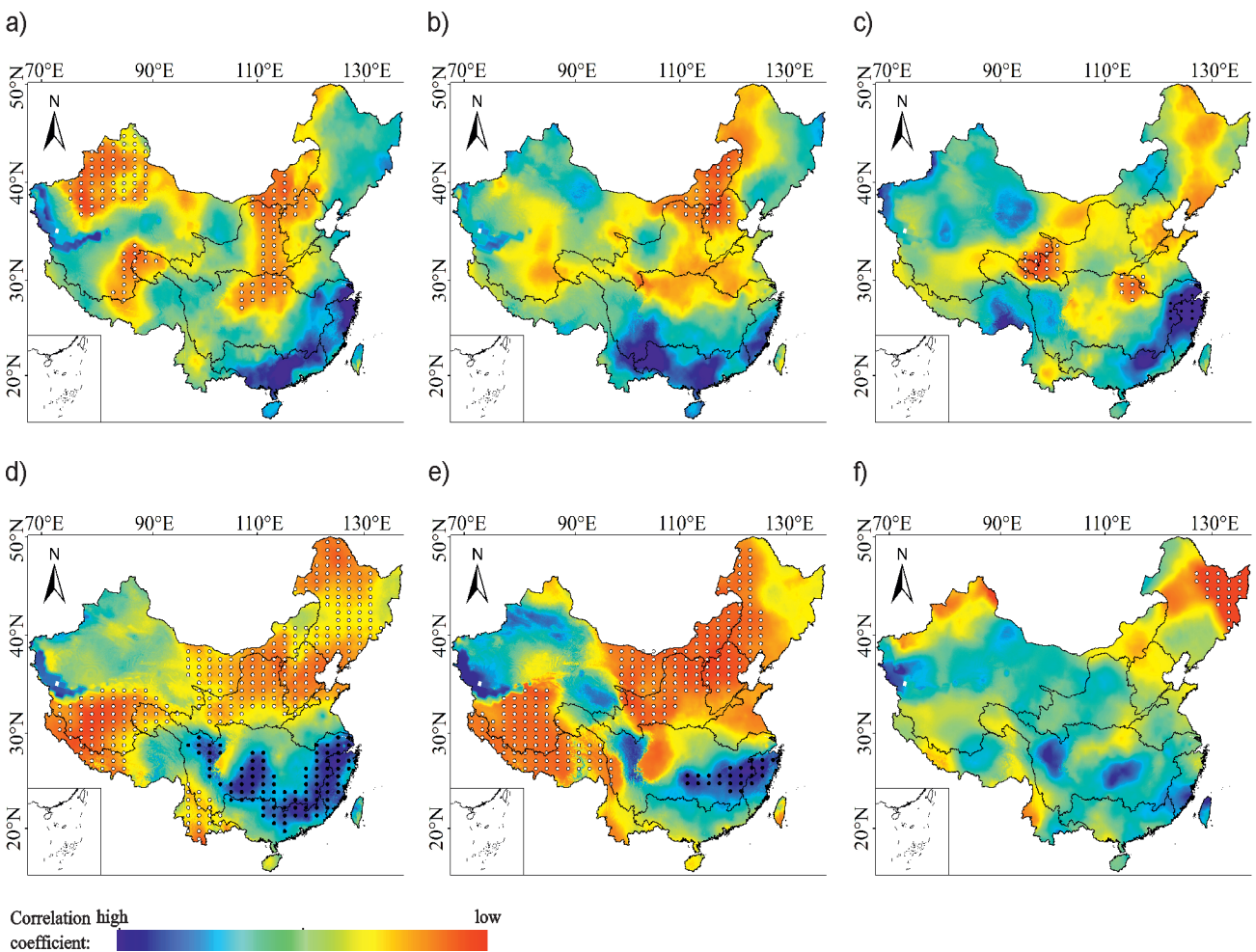


Fig.7. Spatial distribution of correlation coefficient between precipitation and ONI under different ENSO events. Note: The white dots represented significant negative correlation, and the black dots represented significant positive correlation.

under different types and intensities of ENSO events. Since the correlation between precipitation and ENSO events with weak or extremely weak intensity was low overall (e.g., when EW occurred, the absolute value of the correlation coefficient between precipitation and ONI was mostly less than 0.25, which did not pass the significance test), this study was only conducted for extremely strong, strong and medium ENSO events.

As shown in the Fig. 7a) and Fig. 7b), with the occurrence of EES, ES, precipitation and ONI were mainly negatively correlated, and the overall correlation gradually weakened from north to south. The difference was that when EES occurred, precipitation and ONI were strongly negatively correlated in the northwest of the Continental Basin and the east of the Yellow River Basin, the correlation gradually weakened southward and became positive. When ES occurred, the correlation between precipitation and ONI was only strong at the junction of the Continental Basin, the Yellow River Basin and the Haihe River Basin, but weak in the rest of the regions; When LES and LS occurred (Fig. 7(d,e)), the correlation between precipitation and ONI were strong overall, and the areas that passed the 95% confidence level significance test accounted for 77.5% and 55.2% of the total study area, respectively, among which, the areas with significant negative correlation were mainly distributed in the Songhua and Liaohe River Basin, the Yellow River Basin, and the Haihe River Basin, while the Southeast Basin mostly showed significant positive correlation. When EM and LM occurred (Fig. 7(c,f)), the correlation between precipitation and ONI were weak as a whole, and the areas that passed the 95% significance test only accounted for 6.5% and 8.3% of the total area, respectively. The areas with strong

correlation for the former were mainly located in the western part of the Yellow River Basin and the Southeast Basin, while the latter had a strong correlation in the eastern part of the Songhua and Liaohe River Basin.

Discussion

The overall precipitation in the study area was mainly on the rise, accounting for 63.1% of the total study area. The area with decreased precipitation accounted for 36.9%, which was mainly distributed in both sides of the "Huhuanyong Line". and small areas within the Continental Basin. From northwest to southeast, there was a five-layered sandwich structure of "rising-falling-rising-falling-rising" precipitation as a whole (Fig. 8a). In terms of time, the precipitation rose (1900s~1950s), then fell (1960s~1970s) and then rose again (1980s~2010s) (Fig. 8b). This was basically consistent with the conclusion that summer precipitation in the source regions of the Yangtze River and the Yellow River showed slightly increased [45]. The summer precipitation in the study area had main cycles of 110a and 88a, and had 72a and 51a cycles respectively on those two time scales. Scholar Fu Tiewen et al. proposed that there were four types of scale periodic changes in the precipitation sequence in the Guangdong-Hong Kong-Macao Greater Bay Area including 3~8a, 10~15a, 17~23a, and 24~32a [46]. which was different from the result of this paper, and may be caused by different study areas.

There was less precipitation in the study area generally in the year when the ENSO occurred, but there were also differences in event types, intensity, and regions. For example, El Niño had a greater impact on

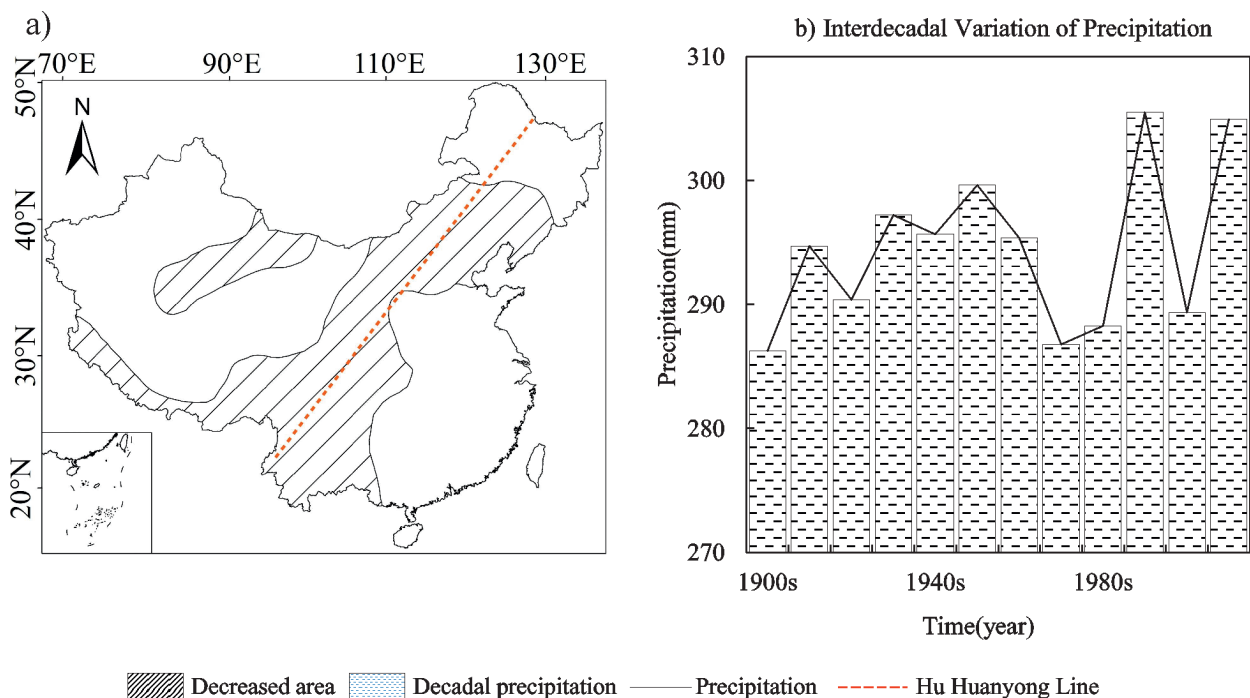


Fig. 8. Spatial and temporal distribution of summer precipitation.

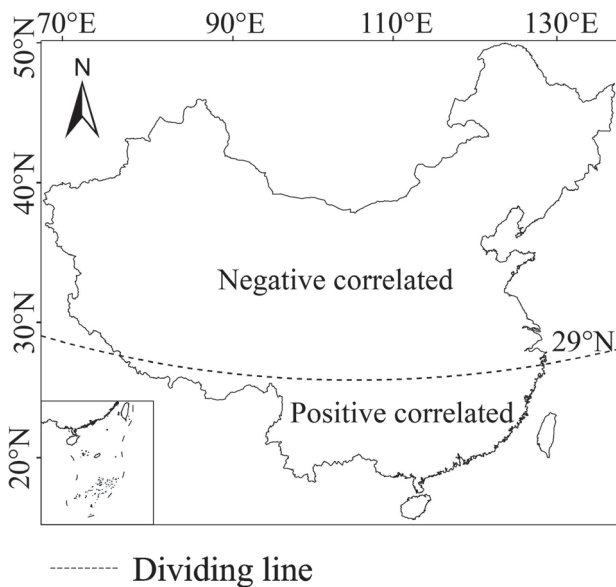


Fig. 9. The dividing line of correlation.

the variation amplitude of precipitation than La Niña. When El Niño (all types) occurred, there was more precipitation in the Continental Basin and the southern Huaihe River Basin, and less in the Yellow River Basin. When the LES and LM occurred, there was more precipitation in the centre while less precipitation in the north and the south of the study area. The difference was that the former's PDSF was between 6% and 14%, while the latter less than 5%. When LW occurred, the precipitation in the study area increased in the northwest and decreased in the southeast, and vice versa for LEW. The conclusions that when El Niño (La Niña) occurred, the precipitation usually increased (decreased) in some regions [47], the precipitation in East Asia, North America and other places in El Niño years was increased by approximately 20% [48] were similar to this article. Some scholars also proposed that ENSO event had no significant impact on precipitation in the Yangtze River Basin, the difference between the conclusion and this paper possibly due to different study periods [49].

Precipitation and ONI were mainly negatively correlated. As a whole, there was a negative correlation in the north (accounting for about 72.9% of the total study area, mainly distributed in the Yellow River Basin, the Songhua and Liaohe River Basin, etc.), and a positive correlation in the south, the dividing line was approximately at 29°N (Fig. 9). On the other hand, the correlation coefficient between precipitation and ONI was proportional to the intensity of the ENSO event. That was, the correlation between precipitation and ONI was strongest under the premise of extremely strong ENSO events occurred, followed by strong ENSO events occurred and medium ENSO events occurred, and the correlation between precipitation and ONI with weak or extremely weak ENSO events occurred did not pass the significance test. The relationship between precipitation

and ENSO in Canada [13], and other places was similar to that in this study area. However Kamil Shahzad et al. Proposed [50] that the winter precipitation in the Western Himalaya-Karakoram-Hindukush region had a significant positive correlation with ENSO in 1986~2015, which was different from the results of this study, and may be caused by the differences in time scales and study area.

Some scholars have also proposed that ENSO can indirectly affect precipitation by affecting Asian summer monsoon [51], tropical cyclones [20] and atmospheric rivers [52], etc., So, the influence mechanism of ENSO on precipitation needs to be further studied in the future. In this article, the temporal and spatial variation of summer precipitation in China and its response to ENSO were analyzed in detail. However, due to the limited length of the time series and limited data, there were uncertainties and limitations in the analysis. This study had a certain reference value for revealing the temporal and spatial changes of precipitation in China and its response to ENSO, and it was all the more conducive to the improvement of the ecological environment, disaster prevention and other aspects.

Conclusions

The precipitation increased in 1900s~1950s, then decreased in 1960s~1970s, and increased in 1980s~2010s again. In terms of space, the precipitation presented a "five-layered sandwich structure" featuring rising-falling-rising-falling-rising" from northwest to southeast. The precipitation was generally lower in the year when ENSO occurred, but there were also differences in ENSO types, intensities, and regions. For example, El Niño had a greater impact on the variation amplitude of precipitation than La Niña did. When El Niño (all types) occurred, there was more precipitation in the western Continental Basin and the southern Huaihe River Basin, but less in the Yellow River Basin. When the LES or LM occurred, the precipitation showed a spatial pattern featuring more precipitation in the central but less in the north and the south, the difference was that the precipitation of the former was mostly reduced by 6% to 14%, and the latter by less than 5%. When the LW occurred, the precipitation increased in the northwest, decreased in the southeast, and vice versa for the LEW. Precipitation and ONI were mainly negatively correlated in time. While in space, there was a negative correlation in the north (accounting for about 72.9% of the total study area, mainly distributed in the Yellow River Basin and the Songhua and Liaohe River Basin, etc.), and a positive correlation in the south, the dividing line was approximately at 29°N. In addition, the correlation coefficient between summer precipitation and ONI was proportional to the intensity of ENSO.

Acknowledgments

This research was funded by the Technology Planning Project of Inner Mongolia (2020GG0074) and the Inner Mongolia Science Foundation (2020MS05054).

Conflict of Interest

The authors declare no conflict of interest.

References

- CHEN D.K., LIAN T. Frontier of El Niño-Southern Oscillation research. *Chinese Science Bulletin*, **65** (35), 4001, **2020**.
- WANG T., LI S.S., YAN J.P., HE J.P. Spatio-temporal variation of summer precipitation in China based on ENSO development process. *Journal of Natural Resources*, **37** (3), 803, **2022**.
- JIAN Y.T., ZHANG B., HUANG H. Regional difference analysis of climate change in Gansu province in recent 58 years and its impact on circulation. *Plateau Meteorology*, **41** (5), 1291, **2022**.
- WANG J.J., SHI B., BAI T., YUAN Q.Y. Spatio-temporal patterns of precipitation and its possible driving factors in the Yellow River Basin. *Journal of Desert Research*, **42** (6), 94, **2022**.
- SHI H.Y., PAN H.S., YANG N., SUN Q. The cause analysis of large-scale circulation of mid-summer precipitation anomalies in Heilongjiang province under ENSO events in 1961-2020. *Journal of Natural Disasters*, **31** (4), 125, **2022**.
- GIOVANNI L., SHAYNE M., MARTIN S., JULIE A., EMANUELE D. Revisiting ENSO and IOD contributions to Australian precipitation. *Geophysical Research Letters*, **49** (1), e2021GL094295, **2022**.
- ROPELEWSKI C.F., HALPERT M.S. Global and regional scale precipitation patterns associated with the El Niño/Southern Oscillation. *Monthly Weather Review*, **115** (8), 1606, **1987**.
- DAI A.G., WIGLEY T.M.L. Global patterns of ENSO-induced precipitation. *Geophysical Research Letters*, **27** (9), 1283, **2000**.
- SOUZA I.P., ANDREOLI R.V., KAYANO M.T., VARGAS F.F., CERON W.L., MARTINS J.A., FREITAS E., SOUZA R.A.F. Seasonal precipitation variability modes over south America associated to El Niño-Southern Oscillation (ENSO) and non-ENSO components during the 1951-2016 period. *International Journal of Climatology*, **41** (8), 4321, **2021**.
- CHEN X., WANG S.S., HU Z.Y., ZHOU Q.M., HU Q. Spatio-temporal characteristics of seasonal precipitation and their relationships with ENSO in central Asia during 1901-2013. *Journal of Geographical Sciences*, **28** (9), 1341, **2018**.
- WEN N., LIU Z.Y., LI L. Direct ENSO impact on east Asian summer precipitation in the developing summer. *Climate Dynamics*, **52** (11), 6799, **2019**.
- CHRISTINE C., SCOTT P. Modelled impact of global warming on ENSO-driven precipitation changes in the tropical Pacific. *Climate Dynamics*, **47** (3-4), 1303, **2016**.
- NALLEY D., ADAMOWSHI J., BISWAS A., GHARABAGHI B., HU W. A multiscale and multivariate analysis of precipitation and streamflow variability in relation to ENSO, NAO and PDO. *Journal of Hydrology*, **574**, 288, **2019**.
- JAI H.L., PIERRE Y.J., SEUNGHO L. Teleconnection of ENSO extreme events and precipitation variability over the United States. *Journal of Hydrology*, **619**, 129206, **2023**.
- AKIYO Y., CHISATO K. Winter orographic precipitation and ENSO in Sapporo, Japan. *Atmosphere*, **13** (1413), 1413, **2022**.
- CHAI R.F. Attribution, prediction and economic and social impacts of global dryness based on CMIP6 model results. *Nanjing University of Information Science and Technology*, **2022**.
- HARUMI S.M., AMBRIZZI T., LIEBMANN B. Extreme precipitation events and their relationship with ENSO and MJO phases over northern South America. *International Journal of Climatology*, **37** (6), 2977, **2017**.
- EMMANUEL I. Linkages between El Niño-Southern Oscillation (ENSO) and precipitation in west Africa regions. *Arabian Journal of Geosciences*, **15** (7), 675, **2022**.
- JOSEPH A.J., BAKER P.L., PETER T.S., CHRISTOPHER T., MARCOS F.A.F., TNAIA I.V., LAURA T. Spatio-temporal patterns of ENSO-precipitation relationships in the tropical Andes of southern Peru and Bolivia. *International Journal of Climatology*, **41** (8), 4061, **2021**.
- DU X.J., INGRID H., LINDA H., ERIK B., ARNDT S., DOROTHY P. Interannual southern California precipitation variability during the common era and the ENSO teleconnection. *Geophysical Research Letters*, **47** (1), **2020**.
- WU R.G., SHI Y., ZHU P.J., JIA X.J. An interdecadal change in august Indochina Peninsula precipitation-ENSO relationship around 1980. *Climate Dynamics*, **60** (1-2), 323, **2023**.
- ZHENG F., WANG H., LUO H., YI S. J. Decadal change in ENSO related seasonal precipitation over southern China under influences of ENSO and its combination mode. *Climate Dynamics*, **54** (3-4), 1973, **2020**.
- PU Y.L., FENG J., LI J.P. Influence of developing phase of eastern pacific El Niño events on the autumn extreme precipitation in China. *Plateau Meteorology*, DOI: 10.7522/j. issn. 1000-0534. 2023. 00004. **2023**.
- LI S.S., DUAN K.Q., WANG T., HE J.P., YAN J.P. Spatio-temporal variation of cold-season snowfall in the south and north of the Qinling Mountains during 1970-2018. *Scientia Geographica Sinica*, **42** (1), 163, **2022**.
- ZHANG Y., ZHOU W., WANG X., WANG X., ZHANG R.H., LI Y.N., GAN J.P. IOD, ENSO, and seasonal precipitation variation over eastern China. *Atmospheric Research*, **270**, 1, **2022**.
- ZHANG R.H., TIAN W.S., HE X., QIE K., LIU D., TIAN H.Y. Enhanced influence of ENSO on winter precipitation over southern China in recent decades. *Journal of Climate*, **34** (19), 7983, **2021**.
- LI J.N., HUANG D.Z., LI F.Z., WEN Z.P. Circulation characteristics of EP and CP ENSO and their impacts on precipitation in south China. *Journal of Atmospheric & Solar-Terrestrial Physics*, **179**, 405, **2018**.
- CHEN L., LI G., LONG H.M., GAO C.J., ZHANG Z.Y., LU B. Interdecadal change in the influence of El Niño in the developing stage on the central China summer precipitation. *Climate Dynamics*, **59** (5-6), 1265, **2022**.

29. CHEN L., LI G. Interdecadal change in the influence of El Niño in the developing stage on the central China summer precipitation. *Climate Dynamics*, **59**, 1981, **2022**.
30. YIN X.X., ZHOU L.T. Strengthened relationships of northwest China wintertime precipitation with ENSO and mid-latitude north Atlantic SST since the mid-1990s. *Journal of Climate*, **33** (10), 3967, **2020**.
31. HAN T.T., WANG H.J., SUN J.Q. Strengthened relationship between eastern ENSO and summer precipitation over northeastern China. *Journal of Climate*, **30** (12), 4497, **2017**.
32. JIA Y.Q., ZHANG B. Correlation analysis of variation of dry-wet climate and ENSO in northern China during 1960-2017. *Scientia Geographica Sinica*, **40** (12), 2115, **2020**.
33. GONG L.L., WANG C.Y., YU Y.C., HAN J.W., WANG X. Multi-scale features of precipitation in the Weichang region Hebei province from 1951 to 2018. *Journal of Water Resources and Water Engineering*, **31** (5), 87, 101, **2021**.
34. DENG H.J., GUO B., CAO Y.Q., CHEN Z.S., ZHANG Y.Q., CHEN X.W., GAO L., CHEN Y., LIU M.B. Spatial and temporal patterns of day-time and night-time precipitation in China during 1961~2016. *Geographical Research*, **39** (10), 2415, **2020**.
35. PENG S.Z. 1-km monthly precipitation data-set for China (1901-2020). National Tibetan Plateau Data Center, **2020**.
36. MA L., WANG J.R., LIU T.X., HUANG X., LIU D.H., LI H.Y. Response relationship between vegetation and climate factors in Horqin sandy land from 2000 to 2012. *Transactions of the Chinese Society for Agricultural Machinery*, **47** (4), 162, **2016**.
37. SHANG S.S., LIAN L.S., MA T., ZHANG K., HAN T. Spatio-temporal variation of temperature and precipitation in northwest China in recent 54 years. *Arid Zone Research*, **35** (1), 68, **2018**.
38. SALEEM A., AWANGE J.L., KUHN M., JOHN B., HU K. Impacts of extreme climate on Australia's green cover (2003~2018): a modis and mascon probe. *Science of the Total Environment*, **766**, 142567, **2021**.
39. LI Y.L., WEN Y.L., LAI H.X., ZHAO Q.Q. Drought response analysis based on cross wavelet transform and mutual entropy. *Alexandria Engineering Journal*, **59** (3), 1223, **2020**.
40. MA Z.G., GUO Q.Y., YANG F.Y., CHEN H.L., LI W.Q., LIN L.L., ZHENG C.Y. Recent changes in temperature and precipitation of the summer and autumn seasons over Fujian province, China. *Water*, **13** (14), 1900, **2021**.
41. WALLACE J.M., GUTZLER D.S. Teleconnections in the geopotential height field during the northern hemisphere winter. *American Meteorological Society*, **109** (4), 784, **1981**.
42. XU Q.T., CHEN L., FAN Y.H., TANG W.W., LU B.H. Relationship between lanzhou drought and climate indices based on SPEI index. *Journal of China Hydrology*, **41** (2), 56, **2021**.
43. HAO Z.X., LIU K.B., ZHANG X.Z., LI M.Q., ZHENG J.Y. Relationship between ENSO episode and the spatial pattern of precipitation in eastern China as simulated in CESM control experiment. *Journal of Natural Resources*, **31** (12), 1984, **2016**.
44. LI X.Y., ZHAI P.M. On indices and indicators of ENSO episodes. *Acta Meteorologica Sinica*, **58** (1), 102, **2000**.
45. LIU X.Q., WU Z.Z., LIU Y.S., ZHAO X.Z., RUI Y., ZHANG J. Spatial-temporal characteristics of precipitation from 1960 to 2015 in the three rivers' head-stream region, Qinghai, China. *Acta Geographica Sinica*, **74** (9), 1803, **2019**.
46. FU T.W., XU Z.X., CHEN H., HUANG Y.X., YE C.L. Analysis on spatio-temporal evolution characteristics of precipitation in Guangdong-Hong Kong-Macao Greater Bay area from 1961 to 2014. *Water Resources Protection*, **38** (4), 56, **2022**.
47. MALESKI J.J., MARTINEZ C.J. Coupled impacts of ENSO AMO and PDO on temperature and precipitation in the Alabama-Coosa-Tallapoosa and Apalachicola-Chattahoochee-Flint river basins. *International Journal of Climatology*, **38** (s1), e717, **2018**.
48. YOUNG M.Y., JAE H.P., SOON-I A., WANG B., LUO X. Mean sea surface temperature changes influence ENSO-related precipitation changes in the mid-latitudes. *Nature Communications*, **12** (1), 1, **2016**.
49. TAMADDUN K. A., KALRA A., BERNARDEZ M., AHMAD S. Effects of ENSO on temperature, precipitation, and potential evapotranspiration of north India's monsoon: an analysis of trend and entropy. *Water*, **12** (1), 1, **2019**.
50. KAMIL S., ALMAZROUI M., KANG I. S., HANIF M., KUCHARSKI F., ABID M.A., SAEED F. Long-term ENSO relationship to precipitation and storm frequency over western Himalaya-Karakoram-Hindukush region during the winter season. *Climate Dynamics*, **53**, 5265, **2019**.
51. WU X.B., LI G., JIANG W.P., LONG S.M., LU B. Asymmetric relationship between ENSO and the tropical Indian Ocean summer SST anomalies. *Journal of Climate*, **34** (14), 5955, **2021**.
52. XIONG Y.T., REN X.J. Influences of atmospheric rivers on north Pacific winter precipitation: climatology and dependence on ENSO condition. *Journal of Climate*, **34** (1), 277, **2021**.